Measurement of the broadband complex permittivity of soils in the frequency domain with a low-cost Vector Network Analyzer and an Open-Ended coaxial probe

Juan D. González-Teruel [a,*], Scott B. Jones [b], David A. Robinson [b,c], Jaime Giménez-Gallego [a], Raúl Zornoza [d], Roque Torres-Sánchez [a]

[a] Department of Automatics, Electrical Engineering and Electronic Technology, Technical University of Cartagena, 30202 Cartagena, Spain
[b] Department of Plants, Soils and Climate, Utah State University, Logan, UT 84322, USA
[c] UK Centre for Ecology & Hydrology, ECW, Bangor LL572UW, UK
[d] Department of Agricultural Engineering, Technical University of Cartagena, 30203 Cartagena, Spain

ABSTRACT

The performance of a handheld Vector Network Analyzer (VNA), the nanoVNA, a low-cost, open-source instrument, was evaluated. The instrument measures the complex permittivity of dielectric media from 1-port reflection parameters in the 1 – 900 MHz bandwidth. We manufactured an open-ended coaxial probe using a SMA-N coaxial adapter to perform dielectric measurements. The accuracy of the nanoVNA was comparable to that of a commercial VNA between 1 and 500 MHz according to tests in reference organic liquids, while a lack of stability was found beyond 700 MHz. The self-manufactured open-ended coaxial probe was subjected to a Finite Element Method (FEM) analysis and its electromagnetic (EM) field penetration depth was determined to be 1.5 mm at 100 MHz, being reduced to 1.3 at 900 MHz and thus demonstrating a frequency-dependent support volume. The broadband complex permittivity of three mineral soils of varied textures was obtained for a range of bulk densities and water contents from dry to water-saturated conditions. The dielectric response of the soils approximated the well-known Topp et al. (1980) equation at high frequencies. At lower frequency however, higher permittivities were exhibited due to dielectric dispersion, which emphasizes the importance of EM-based soil moisture sensor operating frequency when considering sensor calibration or comparing the response of different sensors.

1. Introduction

Soil moisture is of major relevance in agricultural and environmental monitoring, having a direct impact in crop growth and yield, and playing an important role in soil conservation and landscape management. Time Domain Reflectometry (TDR) started to be used to determine the water content of soils from travel-time-based apparent permittivity (K_a), beginning with pioneering works of Hoekstra and Delaney (1974) and Davis and Chudobiak (1975), reaching a turning point with Topp, Davis and Annan's seminal paper (Topp et al., 1980). Since then, the dielectric technique has become a standard method to obtain fast-, reliable- and automated-soil moisture measurements. The electromagnetic-based methods have been used not only to determine the soil moisture, but also other relevant soil physical properties, such as electrical conductivity (EC) (Dalton et al., 1984) or dry bulk density (ρ_b) (Ren et al., 2003).

Frequency domain spectroscopy is increasingly applied in soils and other porous media, as it has been demonstrated to provide valuable insight on how frequency-dependent dielectric phenomena can affect moisture sensor readings (González-Teruel et al., 2020; Skierucha and Wilczek, 2010). It is also a promising approach for the indirect determination of other soil physicochemical parameters, such as ρ_b, matric potential, mineralogy, texture or cation exchange capacity (Wagner and Scheuermann, 2009). As suggested by Reinhard Knöchel in the foreword of Electromagnetic Aquametry (Kupfer, 2004), the use of several dielectric variables, e.g. the amplitude and phase of the EM signal at

---

various frequencies could lead to simultaneous porous media multi-parameter determination. The work done in this regard is still limited and two aspects need to be further developed. On the one hand, it is necessary to build models that relate the dielectric properties in the frequency domain with the physicochemical parameters of interest of the media. The information contained in the dielectric spectrum has not yet been fully explained by theoretical models, and semi-empirical models are a meaningful alternative (Loewer et al., 2016). By applying an inversion approach, Bore et al. (2018) managed to estimate both soil volumetric water content (θ_v) and porosity from a single broadband dielectric measurement, based on the combination of a relaxation model and a mixing equation. Efforts should be focused in this direction, increasing the number of estimable parameters and reducing the computational time in the inversion process. On the other hand, to increase the robustness of these models, extensive datasets relating the complex permittivity of soil samples in the frequency domain, $\varepsilon^*(f)$, with soil physicochemical parameters are needed. The most suitable way to perform broadband complex permittivity measurements in the microwave region is by means of an automatic VNA. However, VNAs and their associated instrumentation are well-known to be expensive (Skierucha et al., 2004), which limits their availability for low-budgets and routine sensing. Additionally, in the case of soil, in-situ measurements are particularly relevant, but the vast majority of VNAs are heavy and bulky, so their use is often restricted to laboratory tests. Thus, it is of interest to work towards development of small-sized devices that allow complex permittivity measurement in the frequency for in-situ applications. The ongoing progress in solid state electronics, with the associated downsizing of components, is enabling the construction of smaller, low-cost and embedded devices (Qiwei et al., 2019).

Only a few works have previously reported the use of low-cost handheld VNAs to measure the broadband complex permittivity of soils (Cross, 2014; Demontoux et al., 2021; Qiwei et al., 2019). Cross (2014) evaluated two low-cost VNA models: VNWA2 and miniVNAPro, showing great $S_{11}^*(f)$ uncertainty between 600 and 800 MHz for the former. The frequency range of operation of these models is 1 kHz–1.2 GHz and 100 kHz–200 MHz, respectively, and the cost is around 500 € each. Qiwei et al. (2019) attached a telescopic VHF radio antenna to a miniVNA Tiny, but the study was limited to obtain the broadband electrical resistance of soil as a function of θ_v. The miniVNA Tiny operation frequency range is 1 MHz–3 GHz and it costs around 500 €. Reistad (2018) also used the miniVNA to obtain the dielectric properties of snow. Demontoux et al. (2021) developed a device for continuous in-situ measurements of soil profiles permittivity using a low-cost VNA, but the model is not provided and the cost of the equipment is reported to be around 700 €.VNAs allow us to obtain $\varepsilon^*(f)$ of a sample cell from the complex $S_{11}^*(f)$ parameter (one-port measurement), based on the amplitude and phase of the measured signal in comparison with a reference signal. Coaxial-line cells have become popular in frequency-domain applications to measure the complex permittivity of a sample in a broad bandwidth from about 1 MHz to 40 GHz (Kaatze, 2013). The open-ended coaxial probe is a particular case of coaxial-line cells, which was first used for broadband dielectric property determination of biological tissues and liquids (Marsland and Evans, 1987; Tanabe and Joines, 1976), and subsequently adapted to soil applications (Estevez and Jones, 2009; González-Teruel et al., 2020; Wagner et al., 2014), providing non-destructive measurements and a simple handling of the samples (Kaatze, 2013).

The aim of this paper is to evaluate the performance of a new open-source, low-cost, handheld VNA for the measurement of the broadband complex permittivity of soils at different water contents with a considerably reduced cost in comparison to those used previously with the same aim (Cross, 2014; Demontoux et al., 2021; Qiwei et al., 2019). To do so, we designed and manufactured an open-ended coaxial probe, machined from a standard SMA-N coaxial adapter (González-Teruel et al., 2021). The open-ended coaxial probe has already been successfully validated in the 50–900 MHz frequency range to measure the

complex permittivity of organic reference liquids. Laboratory measurements, based on the determination of the real part of the complex permittivity, $\varepsilon'(f)$, of 1 and 2 mm diameter glass bead packing and their theoretical effective permittivity, $\varepsilon_{eff}(f)$, determined that the EM field penetration depth of the probe was between 1 and 2 mm, limiting its application to fine-grained media (González-Teruel et al., 2021) with diameters below the glass beads tested. In this study, we also complement this finding, which is based on some theoretical assumptions, by performing a 3D FEM analysis.

2. Materials and methods

2.1. Dielectric measurements

To obtain the complex permittivity of the soil in the frequency domain, $\varepsilon^*(f)$, we used a low-cost VNA. There has been a series of releases of low-cost, handheld models of VNAs under the root name nanoVNA ("NanoVNA | Very tiny handheld Vector Network Analyzer," n.d.). The original model of the nanoVNA was designed by the github user edy555 ("edy555 (TT) · GitHub," n.d.) to work in the 50 kHz to 300 MHz frequency range by using a si5351 clock generator. This model was upgraded, under the name nanoVNA-H, by the github users hugen79 ("GitHub - hugen79/NanoVNA-H," n.d.), who extended the frequency range to 900 MHz by improving the frequency algorithm to use the odd harmonic extension of the si5351, and cho45 ("cho45 (Satoh, Hiroh) · GitHub," n.d.), who implemented TDR functionality. Several versions of the nanoVNA-H have been issued, the latest ones (rev3.4, rev3.5 and 4) being able to provide useful measurements up to 1.5 GHz. The nanoVNA is an open-source project and extensive resources are available to reproduce it ("edy555 (TT) · GitHub," n.d., "GitHub - hugen79, Nano-VNA-H," n.d.). The different versions are commercialized overall for<100 €. All versions have two ports (reflection and transmission) implemented with SMA connectors, touch screen, one and two-port calibration functionality with the possibility of storing and recalling the calibration coefficients, and varied formats to present the S-parameters. The reader is referred to ("NanoVNA | Very tiny handheld Vector Network Analyzer," n.d.) for further detail. There is also a new project, which is independent of the one described above, that has released several models under the name NanoVNA V2 or S-A-A-2, reaching up to 3 GHz in the version V2 Plus and up to 4.4 GHz in versions Plus 4 and Plus 4 Pro. However, only version V2.2 resources are available for the reproduction of these models, and is limited for commercial use. In this study, a nanoVNA-H was tested for $\varepsilon^*(f)$ determination from one-port measurements. The original firmware was upgraded to version 0.7.0 – 2020.02.23 – 2.

To evaluate the performance of the nanoVNA for measuring the $S_{11}^*(f)$, a commercial model Agilent 4395A (Agilent Technologies, Inc., Palo Alto, CA, USA) with the 43961A RF Impedance Test Kit to measure one-port S-parameters was used for comparison in the 1–500 MHz frequency range. A LMR-240 UF coaxial cable with SMA (Male-Female) ends connected the reflection port with an open-ended coaxial probe for both VNAs. In the case of the Agilent 4395A, an APC-7 to SMA adapter was required to connect the cable to the 43961A fixture. Both VNAs were one-port calibrated using Open, Short and Load (50 Ω) (OSL) standards at the interface plane between the coaxial cable and the open-ended coaxial probe.

The nanoVNA project also embraces the development of interfaces that enable the nanoVNA's measurements to be controlled and recorded from a PC, or even from a smartphone via a USB cable. Several applications are available to be used in combination with the nanoVNA to perform $S_{11}^*(f)$ data acquisition. We used the nanoVNA-Saver v0.2.2–1 ("GitHub - NanoVNA-Saver," n.d.) for convenience and the frequency sweep was configured from 10 kHz to 900 MHz in nine fragments of 101 points each. The Agilent 4395A was also connected to a PC through a General Purpose Interface Bus (GPIB) and $S_{11}^*(f)$ parameters were recorded with IntuiLink software (Keysight Technologies, Santa Rosa,

CA, USA) in Microsoft Excel (Microsoft Corporation, Redmond, WA, USA). The excitation was configured from 1 MHz to 500 MHz in one fragment of 500 equidistant points.

2.1.1. Open-Ended coaxial probe calibration

The open-ended coaxial probe used in this study, hereinafter termed the OE probe, was described and evaluated in González-Teruel et al. (2021). The probe inner conductor diameter is 2.3 mm, whereas the inner and outer diameters of the outer conductor are 7.3 and 12, respectively. To obtain $\varepsilon^*(f)$ from $S_{11}^*(f)$ measurements with an open-ended coaxial probe, semi-analytical and empirical approaches can be found in the literature (Marsland and Evans, 1987; Mosig et al., 1981). The complex admittance, Y^*, of an open-ended coaxial line radiating into an infinite dielectric can be expressed as a function of the complex reflection coefficient, Γ^* (García-Baños et al., 2005):

$$Y^* = \frac{1 - \Gamma^*}{1 + \Gamma^*} \tag{1}$$

At low frequencies, Y^* can be replaced by the admittance of the open-ended coaxial probe lumped equivalent circuit (Stuchly et al., 1982), depicted in Fig. 1.

Mosig et al. (1981) derived an integral equation for broadband analysis that takes into account the effects of radiation and of higher order modes. Although there is no analytical solution, numerical methods may be applied to solve it. Nevertheless, the $S_{11}^*(f)$, which is directly obtained with the VNA, does not correspond exactly with Γ^* because the actual reflection coefficient and $S_{11}^*(f)$ include error effects from the coaxial line and connectors (Stuchly et al., 1982; Wagner et al., 2014). To eliminate these systematic errors an empirical calibration must be performed. Alternatively, fully empirical approaches avoid possible errors that can result from theoretical assumptions and inaccuracies in the determination of the geometrical characteristics of the probe, making use of a bilinear equation to establish a relationship between $S_{11}^*(f)$ and $\varepsilon^*(f)$ from the known properties of reference materials (Estevez and Jones, 2009; Kraszewski et al., 1983; Marsland and Evans, 1987; Wagner et al., 2014). Thus, this equation can be expressed as:

$$\varepsilon^*(f) = \frac{c_1^*(f)S_{11}^*(f) - c_2^*(f)}{c_3^*(f) - S_{11}^*(f)} \tag{2}$$

where $c_1^*(f)$, $c_2^*(f)$ and $c_3^*(f)$ are frequency dependent complex coefficients. Considering that the reference materials are air, water and another reference liquid, Wagner et al. (Wagner et al., 2014) derived the equations for the Open, Water, Liquid (OWL) calibration:

Fig. 1. Open-ended coaxial probe radiating into a MUT (Material Under Test) with unknown effective permittivity ε_{eff}^* and lumped equivalent circuit, where C_f is the capacitance of the teflon-filled part of the coaxial line and C_0 (ε_{eff}^*) and G (ε_{eff}^*) represent the fringing field radiation into the MUT.

$$\begin{aligned} S_{11,O}^*(f)c_1^*(f) - c_2^*(f) - \varepsilon_O^*(f)c_3^*(f) &= -\varepsilon_O^*(f)S_{11,O}^*(f) \\ S_{11,W}^*(f)c_1^*(f) - c_2^*(f) - \varepsilon_W^*(f)c_3^*(f) &= -\varepsilon_W^*(f)S_{11,W}^*(f) \\ S_{11,L}^*(f)c_1^*(f) - c_2^*(f) - \varepsilon_L^*(f)c_3^*(f) &= -\varepsilon_L^*(f)S_{11,L}^*(f) \end{aligned} \tag{3}$$

where subscripts O, W and L denote Open, Water and Liquid, respectively. By solving the system of equations in (3), from the measurement of $S_{11}^*(f)$ in the three standards and knowing their corresponding $\varepsilon^*(f)$, the calibration coefficients are determined. Then, $\varepsilon^*(f)$ can be estimated from (2) using new $S_{11}^*(f)$ measurements. Nonetheless, Wagner et al. (2014) reported limitations of the OWL method with the open-ended coaxial probe and a VNA below 50 MHz on the estimation of $\varepsilon'(f)$ for electrically lossy materials when using electrically lossless materials as Liquid standard and proposed the Open, Water, Short (OWS) method as an alternative for that bandwidth. However, experimental limitations are encountered when trying to provide a shorting empirical standard for non-commercial probes.

2.2. OE probe 3D FEM analysis

To precisely determine the EM field penetration depth of the OE probe, it was subjected to a FEM analysis. The 3D model of the OE probe was built from the CAD file of the original coaxial SMA-N adapter provided by the manufacturer (Telegärtner Karl Gärtner GmbH, Berlin, Germany) and imported to SolidWorks (Dassault Systèmes SolidWorks Corporation, Waltham, MA, USA), where the machining made on the actual probe was replicated. Then, the 3D model was imported to CST Microwave Studio software (Dassault Systèmes SolidWorks Corporation, Waltham, MA, USA), as shown in Fig. 2, where the FEM analysis was carried out. The probe materials were defined as Brass (65%) for the inner and outer conductors, and PTFE (lossy) for the coaxial dielectric, selected from the software predefined materials list. The simulations were run from 10 kHz to 900 MHz by using the Time Solver. The excitation discrete port was set at the plane where the actual probe would match the coaxial cable, presented as the red-dotted face in Fig. 2b. The FEM software provides $S_{11}^*(f)$ by solving Maxwell's equations from the hexahedral mesh of the 3D model.

Meaney et al. (2016) proposed an empirical method to determine the effective field penetration depth of an open-ended coaxial probe by using a two-layer MUT, and quantifying the contribution of the two layers to the bulk measurement when varying the thickness of the layer in contact with the probe (layer 1), d. They used water for layer 1 and either a Teflon or acrylic cylinder for the other layer (layer 2) and obtained the MUT effective permittivity as a function of d. Thus, when d is close to zero, the relationship between MUT effective permittivity and d is practically linear, with the curve tending asymptotically to the permittivity of the material of layer 1 as d is increased. The criterion to define the effective field penetration depth was set as the value of d for which the effective permittivity measured with the probe drops "20% below that of the ideal straight line extrapolated from the straightest section of the curve beginning at exact contact". In turn, the straightest section of the curve, beginning from $d = 0$, was defined as the longest possible where a straight line fit would yield an R^2 of at least 0.99.

In this study, we followed the method proposed by Meaney et al. (2016) and applied it through the OE probe FEM simulations to determine its effective EM field penetration depth. The probe was immersed in a two-layer 10 mm × 10 mm × 13 mm square prism. The material of layer 1 was defined as distilled water and that of layer 2 as air, as shown in Fig. 2c, where layer 1 is presented in blue and layer 2 in yellow. The thickness of layer 2, h, was swept from 2 mm to 9 mm in 1 mm steps and more finely from 9 mm to 10 mm in 0.1 mm steps, while keeping $d + h = 10$. The maximum mesh cell size was set to 20 cells per wavelength and the minimum to a fraction of 20 of the maximum cell. Since near the open end of the probe a higher resolution is required to refine the estimation of the effective field penetration depth, 10 additional cells
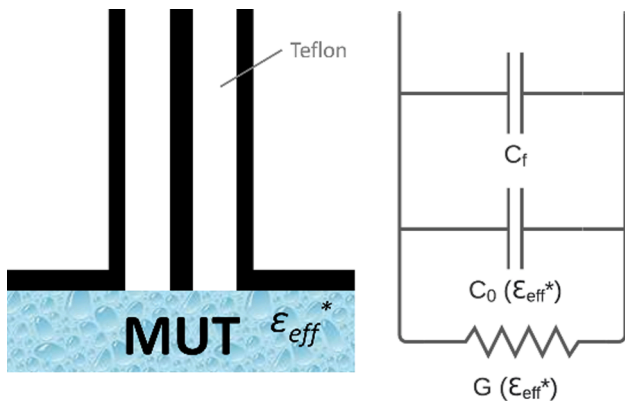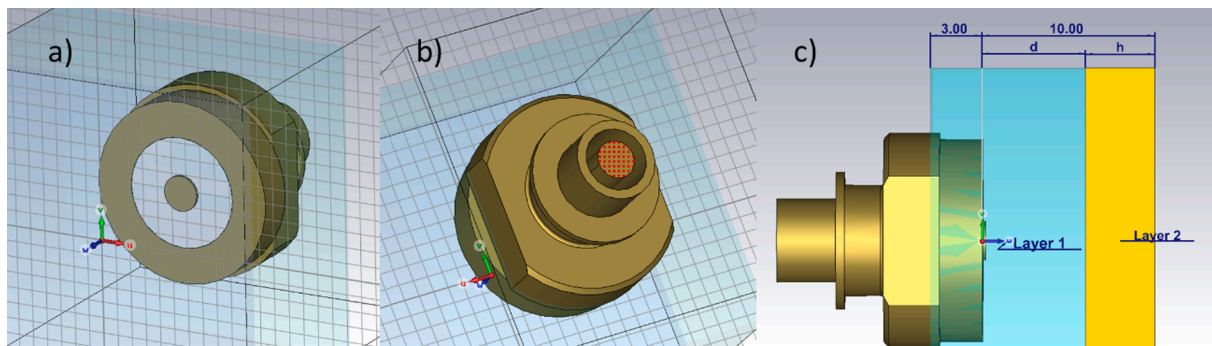
Fig. 2. a) open-ended plane, b) measurement port plane and c) MUT layer configuration views of the OE probe 3D model. Dimensions in mm.

around the model edges were set, as well as 3 additional fine cells around the model box, considering the materials properties for mesh refinement. In order to calculate $\varepsilon^*(f)$ from simulated $S_{11}^*(f)$, the OWL method described in section 3.1.1 was applied, using acetone as the Liquid standard. The reference $\varepsilon^*(f)$ values of acetone, as well as of other standard liquids used in this study are provided in the next section.

2.3. Calibration and test media

2.3.1. Calibration materials

To calibrate the OE probe by applying the OWL method, three reference media are needed. For the Open standard, the probe was set to measure in air, whose $\varepsilon^*(f)$ was approximated to that of a vacuum, with a constant value of 1 in the frequency domain. For the Water standard, ultrapure water (type 1 water according to ASTM D1193 – 06 (ASTM, 2018)) was used. For the Liquid standard, several high purity organic liquids have been used in the literature. Following the procedure described in González-Teruel et al. (2021), we used acetone, iso-propanol, methanol and ethylene–glycol (99%), with 99, 98.5, 96 and 99% purities, respectively, covering a wide range of permittivity values. Several iterations were made by using one of these four liquids as the Liquid standard and leaving the others to test the accuracy of the cali-bration. Reference $\varepsilon^*(f)$ values of the liquids were obtained from the literature, according to different dielectric relaxation models. The ul-trapure water $\varepsilon^*(f)$ was modelled with the Debye equation (Debye, 1929) from data in Kaatze (1989); acetone with the Cole-Cole equation (Cole and Cole, 1941) from data in (Buckley and Maryott, 1958), and methanol, isopropanol and ethylene–glycol with the Debye, double Debye and Havriliak-Negami equations (Havriliak and Negami, 1967), respectively, from Gregory and Clarke (2012).

To perform the $S_{11}^*(f)$ measurements, the OE probe was immersed in the standard liquids, placed in a beaker, as shown in Fig. 3. The average of three measurements was considered. Between liquids, both the probe and the beaker were cleaned with acetone to avoid cross contamination of the successive media. To ensure that the probe was cleaned, a check measure in air was made after every liquid and compared to a pre-trial one. The calibration of the OE probe was made at 22–23 °C. To measure the temperature of the calibration and test fluids, we used a thermo-couple Type K Comark C28 (Comark Instruments, Norwich, Norfolk, UK). Since the parameters of the relaxation models in the literature are provided either in 5 or 10 °C steps, their values between 22 and 23 °C were linearly interpolated.

2.3.2. Soils

Disturbed samples of three different mineral soils collected from the Region of Murcia, Spain, were used in this study. The soils tested were a Sandy Clay Loam Haplic Calcisol, a Clay Loam Haplic Calcisol, and a Silt Haplic Calcisol (Anjos et al., 2015). The soils' particle size distribution is specified in Table 1 for samples sieved to below 2 mm, as well as other representative physico-chemical properties. In order to ensure a
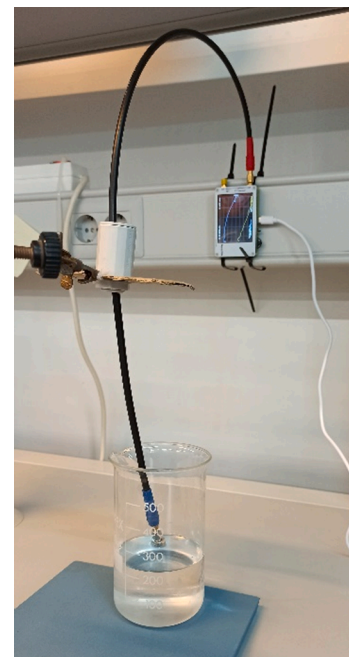

Fig. 3. Standard liquids $S_{11}^*(f)$ measurement setup.

minimum number of soil particles in the limited volume of influence of the OE probe to obtain representative measurements, the soils were sieved to below 0.2 mm (UNE-7050–3).

2.4. Granular media test method

A cylindrical sample holder with an inner diameter of 29 mm and height of 30 mm, shown in Fig. 4, was designed *ad hoc* and manufac-tured with a 3D printer to perform the measurements in granular ma-terials. The holder was designed to place the probe at the bottom, facing upwards, letting the granular sample lie on the probe by gravity providing good contact, also avoiding the sample disturbance and un-desirable extra packing caused if the probe was inserted from the top into the sample.

Soil samples were prepared by spraying different volumes of distilled water on disturbed air dried samples and mixed thoroughly, then packed uniformly into the sample holder, gradually increasing ρ_b, and per-forming the dielectric measurements at every packing. Thus, multiple moisture and density conditions were obtained for the same sample. Depending on soil moisture, the packing depth of the samples ranged from 9 to 13 mm and the initial mass of the dry sample was kept to 9.65 g for every sample, so that we were able to set ρ_b from 1.1 to 1.6 g cm^{-3}. Samples were packed by means of a depth-graduated cylinder with an

Table 1
Soil sample texture by particle size (USDA), pH and electrical conductivity (EC) of the 1:5 saturation extract and the Cation Exchange Capacity (CEC) of each sample.

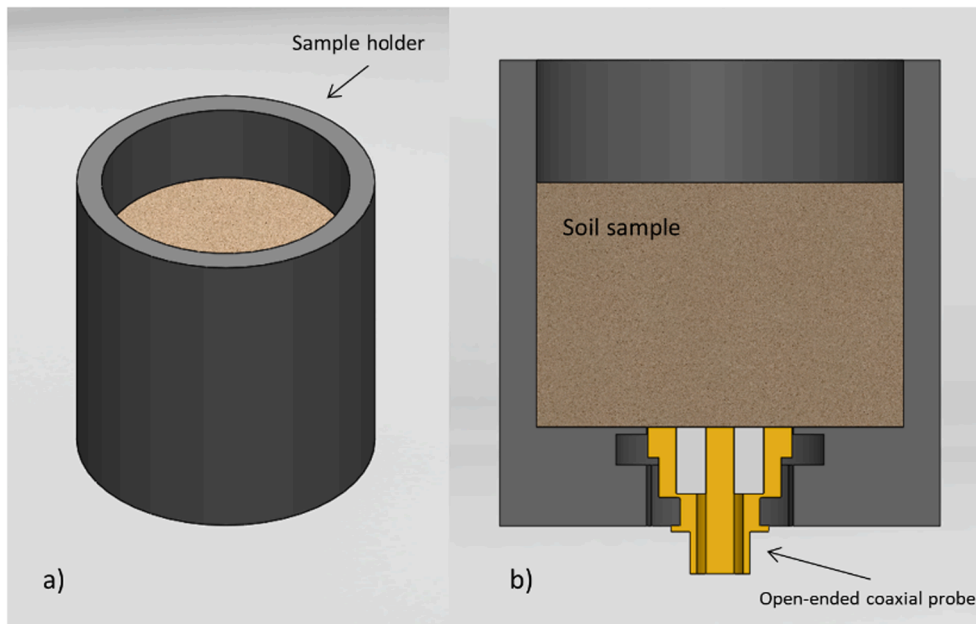| Soil	Texture	Particle size distribution			pH	EC 1:5 @ 23 °C (dS/m)	CEC (cmol/kg)
		Sand (%) (2000–50 µm)	Silt (%) (50–2 µm)	Clay (%) (<2 µm)			
Haplic Calcisol	Sandy Clay Loam	49.55	20.00	30.45	8.7	1.000	14.6
Haplic Calcisol	Clay Loam	39.15	27.50	33.35	8.2	0.217	19.0
Haplic Calcisol	Silt	7.79	85.36	6.38	8.5	0.225	17.4

Fig. 4. Designed sample holder with the OE probe placed at the bottom and a soil sample. (a) Perspective view; (b) section view.

outer diameter that fitted tightly into the inner diameter of the sample holder. An average from three repetitions of the dielectric measurements was recorded for every packing. Soil water content was determined by following the thermo-gravimetric method after removing the soil from the sample holder and oven-drying at 105 °C during 24 h.

3. Results and discussion

3.1. nanoVNA assessment

3.1.1. Agilent 4395A and nanoVNA comparison

To evaluate the performance of the nanoVNA for dielectric measurements, initially we have focused the analysis on the $S_{11}^*(f)$ data, as it is a raw parameter obtained directly from the VNA, which allows a fair comparison between VNA devices. In Fig. 5, we compare the real (5a) and imaginary (5b) parts of the $S_{11}^*(f)$ measured with the nanoVNA (solid lines) and the Agilent 4395A (dotted lines) in the test fluids
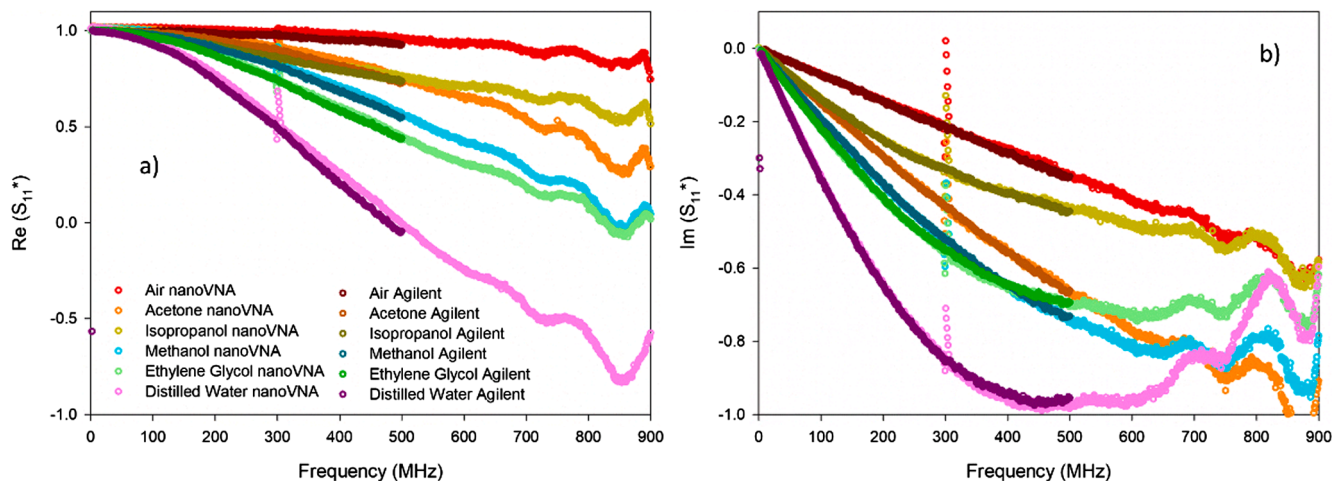

Fig. 5. Real (a) and imaginary (b) parts of the $S_{11}^*(f)$ determined in the test fluids with the nanoVNA (solid lines) and the Agilent 4395A (dotted lines).

described in section 2.3.1. The frequency range of the Agilent 4395A is limited to 500 MHz, whereas for the tested version of the nanoVNA, the maximum EM frequency is 900 MHz. The data obtained with both VNAs are very close for each fluid sample, especially in the case of the imaginary part, where the data practically overlap. In the real part, although there are no significant differences between the two VNAs, differences become more evident from 300 MHz and above. This frequency value, from which the measurements of the nanoVNA are not directly obtained by hardware, but derived from harmonic extensions, seems critical, since the data shows an unexpected peak in the spectrum, similar to the effect generated by a resonance. Nonetheless, the repeatability of this phenomenon, always observed in the same 296–306 MHz narrow bandwidth, is easily amendable by removing the corresponding data and applying an interpolation. Beyond 500 MHz there are no data from the Agilent 4395A to compare, but we note that beyond 700 MHz the nanoVNA data become noisier and show an oscillation whose amplitude increases as the permittivity of the fluid does. According to Gregory and Clarke (2007), flange resonances occur (approximately) when measuring high permittivity liquids with tan δ < 0.3, where the loss tangent is defined as tan $\delta = \varepsilon'' / \varepsilon'$. The frequency at which these resonances show up is related with the open-ended probe diameters, being higher as the smaller the dimensions of the probe are. For a probe with a flange inner diameter of 15.1 mm and outer diameter of 50 mm immersed in water, the lowest frequency resonance occurs at approximately 580 MHz, whereas for a flange inner diameter of 7 mm and outer diameter of 25 mm, the resonance occurs at around 1.1 GHz and is much weaker (Gregory and Clarke, 2007). In the case of the open-ended probe used in this study, the inner diameter of the flange is close to 7 mm, but the outer diameter is only about 12 mm, likely shifting flange resonances to frequencies higher than 1.1 GHz. Therefore, the harmonic approximation method implemented to estimate the $S_{11}*(f)$ parameters beyond 300 MHz in the nanoVNA could likely be causing this oscillating effect.

3.1.2. Estimation of the complex permittivity of reference liquids

From the $S_{11}*(f)$ data presented above, we applied the OWL calibration method described in Section 2.1.1. In order to compute a numerical comparison between the two VNAs tested, the nanoVNA data were rescaled to the frequency steps configured in the Agilent 4395A and $S_{11}*(f)$ data were obtained by linear interpolation. We performed the OWL calibration by rotating the organic reference liquids described in Section 2.3.1, using each of them as the Liquid standard in every iteration, while keeping the rest for validation and accuracy assessment. In Table 2, the RMSE, calculated from the estimated real, $\varepsilon'_m(f)$, and imaginary, $\varepsilon''_m(f)$, permittivities after the OWL calibration and the literature reference values ($\varepsilon'_{ref}(f)$, $\varepsilon''_{ref}(f)$) of the organic liquids is reported. For the Agilent 4395A, the lowest error in the real part was achieved with methanol as the Liquid standard, and isopropanol in the imaginary part, being methanol nearby. In the case of the nanoVNA, the lowest error in the real part was found with acetone as Liquid standard, followed closely by ethylene–glycol and methanol. In the imaginary part, acetone, ethylene–glycol and methanol show similar results as well, methanol being the most accurate option. This is in accordance

with the choice of Wagner et al. (2014b), who successfully used pure methanol as the Liquid standard from 50 MHz.

Using methanol as the Liquid standard, in Fig. 6, the real (6a) and imaginary (6b) parts of the estimated complex permittivity with both VNAs and the literature reference values are presented from 1 MHz to 500 MHz for the Agilent 4395A and from 1 MHz to 900 MHz for the nanoVNA. The estimated values of methanol and distilled water match with their references, as they were used for the calibration. The estimates with both devices are broadly in line with the reference values. In Fig. 7, the relative error between the estimated and reference permittivity is presented for both real and imaginary parts in each of the test liquids. The dark shaded areas, encompassing 10–50 MHz and 700–900 MHz, represent the bandwidths where the measurement sets have shown accuracy limitations generally, whereas the light shaded region limits the bandwidth where the nanoVNA measurements are obtained by hardware, together with the 10–50 MHz region. The larger RMSE obtained by the Agilent 4395A in comparison with the nanoVNA, as reported in Table 2, most likely comes from low frequencies (<100 MHz), where the real part of the permittivity is more scattered than that obtained with the nanoVNA, as shown in Fig. 6. This is very likely related to use of the APC-7 to SMA adapter between the Agilent 43961A fixture and the coaxial cable. This adapter was not needed for the nanoVNA and is thus a potential source of uncertainty. This scattering is not observable in Fig. 7, since relative errors higher than 15% are out of the range presented. Nonetheless, the considerable difference between VNAs in the relative error of the real part with isopropanol and acetone, and that of the imaginary part with ethylene glycol, also evidences the marked difference in the RMSE.

According to Fig. 7, the estimation of $\varepsilon'(f)$ is more stable than that of $\varepsilon''(f)$, showing that the latter has higher and more dispersive relative errors. It is also noticeable that the relative error of the real part increases as the frequency does in isopropanol and ethylene glycol, but keeps relatively constant in acetone. This can be explained by the non-relaxing $\varepsilon'(f)$ response of acetone and methanol in the studied bandwidth, in contrast with the dispersion shown by isopropanol and ethylene glycol, so that as the used calibration standards are non-lossy, the model 'struggles' with estimating the dielectric spectra of lossy materials. This could also be extended to the imaginary part, where isopropanol and ethylene glycol dielectric dispersion is markedly different to that of the calibration standards. In the case of acetone, relative errors are markedly larger than the errors in the rest of the testing liquids. Fig. 6 illustrates that the imaginary permittivity of acetone is very proximate to zero for the studied bandwidth, which magnifies the relative error. Additionally, the relative error of the real part of acetone shows increasing values beyond 700 MHz. This also suggests a partial influence of the oscillating behaviour of the nanoVNA $S_{11}*(f)$ measurements in this frequency range, reported above. Summarizing, the relative errors found in the imaginary part are considerably higher than that in the real part, which can be explained by a greater influence of the absolute error at lower $\varepsilon*(f)$ values.

Below 50 MHz, the $S_{11}*(f)$ for the tested media converges to 1 and 0 in case of the real and imaginary parts, respectively, making the open-ended probe paired with a VNA not sensible enough in this bandwidth when applying the OWL calibration. Up to 300 MHz, the nanoVNA shows more stability and consequently more accuracy in the estimations of $\varepsilon'(f)$, with maximum relative errors of 2%. In the frequency range between 300 MHz and 700 MHz, where the nanoVNA estimates the $S_{11}*(f)$ from odd harmonic extensions, based on the measurements up to 300 MHz, the relative error in the real part reaches up to 9% in isopropanol and up to 6% in ethylene glycol. In the imaginary part, the more stable response of the nanoVNA up to 300 MHz is masked by the OWL method associated limitations, related with the differences in the imaginary part relaxation in this bandwidth between the calibration media and that of isopropanol and ethylene glycol. In the case of acetone, the close to zero value of $\varepsilon''(f)$ makes the relative error much greater.
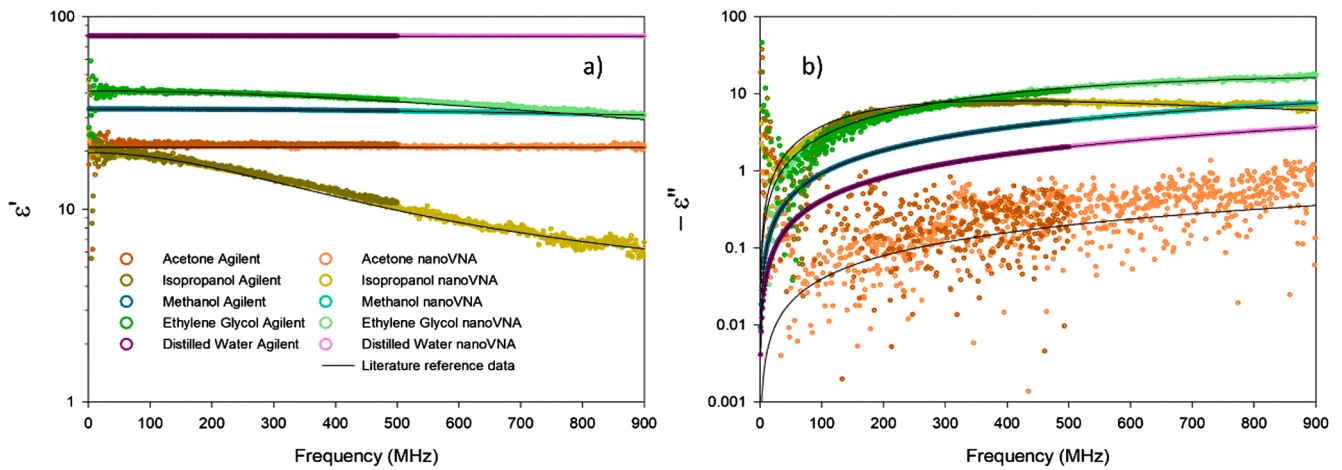
Table 2

RMSE of the OE probe's estimation of the real and imaginary parts of the permittivity on the organic reference liquids not used as standard with the OWL calibrations, which reference literature values for these liquids (Buckley and Maryott, 1958; Gregory and Clarke, 2012).

VNA model	$\varepsilon*$ component	Organic liquid standard			
		Acetone	Isopropanol	Methanol	Ethylene-glycol
Agilent 4395A	ε'	3.3878	2.6476	2.4297	2.8792
	ε''	5.2261	2.2081	2.6840	3.3410
nanoVNA	ε'	0.5723	0.7392	0.6029	0.5924
	ε''	0.5632	0.9760	0.5482	0.5609

Fig. 6. Estimations of ε'(f) and ε''(f) with nanoVNA (light colors scatterers) and Agilent 4395A (dark colors scatterers) based on the OWL calibration compared with the reference values (solid lines) obtained from the literature for the tested fluids at 22–23 °C.
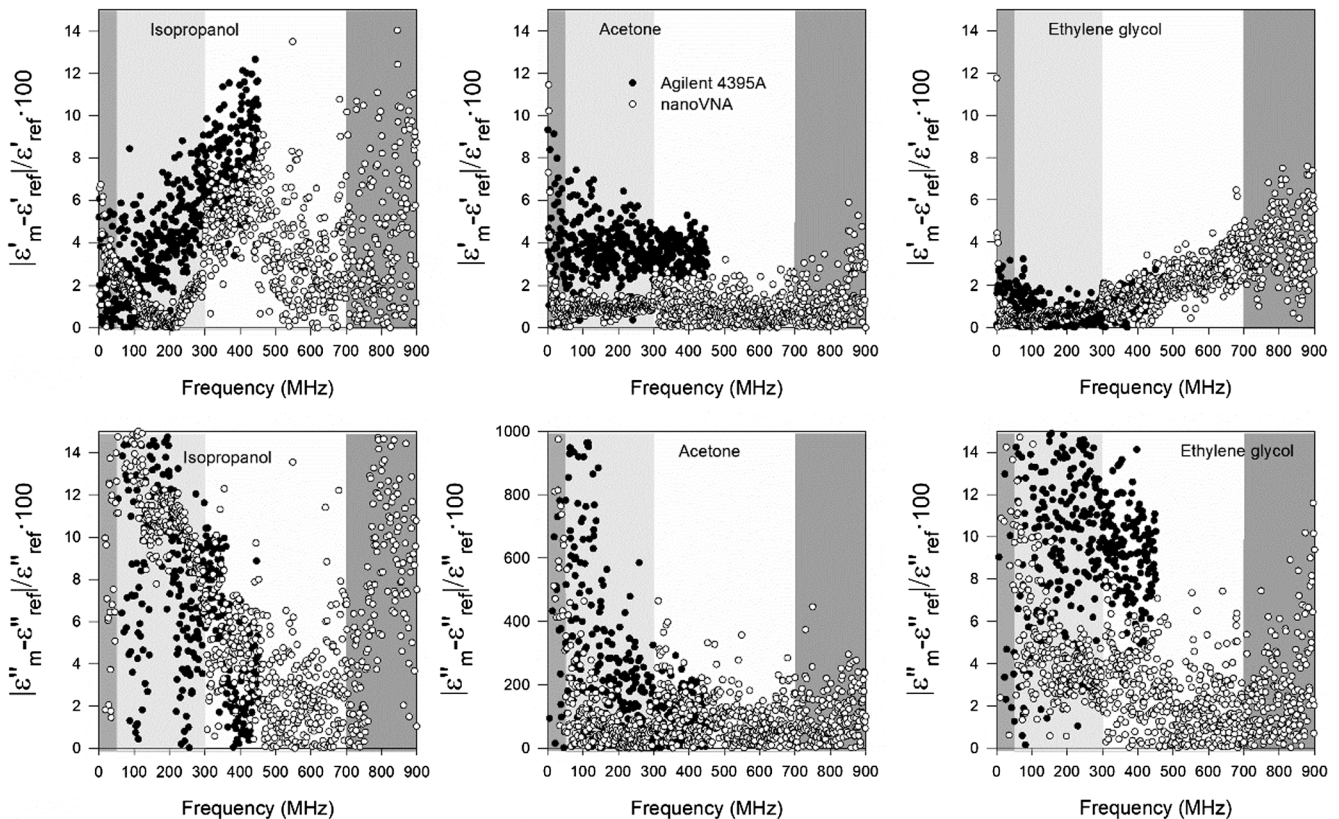

Fig. 7. Relative error (%) of ε'(f) (top) and ε''(f) (bottom) estimations in isopropanol, acetone and ethylene glycol after the OWL calibration using methanol as Liquid standard.

All of this reveals that there is an optimum bandwidth to obtain reliable measurements using the coupled OE probe and nanoVNA between 50 and 700 MHz. In order to identify the most suitable calibration standards combination for this bandwidth, we present the RMSE between the estimated and literature permittivities of the organic liquids for the 50–700 MHz bandwidth in Table 3. Again, isopropanol shows the greatest RMSE, both for the real and imaginary parts, whereas methanol and ethylene–glycol exhibit the lowest RMSE, thus finally selecting the former to determine the complex permittivity of new samples, in accordance with Wagner et al. (2014).

3.2. OE probe EM field penetration depth

In order to determine the EM field penetration depth of the OE probe, $S_{11}{}^{*}(f)$ numerical FEM calculations were obtained in air, distilled water, acetone and methanol and found that the relative error between numerical computations and empirical measurements with the Agilent 4395A were lower than 2%. Therefore, we assumed the actual probe was accurately modelled.

Following the procedure described in Meaney et al. (2016), in Fig. 8 the example of calculation to determine the effective EM field penetration depth of the OE probe is presented for 100 MHz. Numerical

Table 3

Root Mean Square Error (RMSE) of the OE probe and nanoVNA estimation of the real and imaginary parts of the permittivity comparing the organic reference liquids not used as standard with the Open-Water_Liquid (OWL) calibrations within the 50–700 MHz bandwidth, which employs reference literature permittivity values for these liquids (Buckley and Maryott, 1958; Gregory and Clarke, 2012).

ε^* component	Organic liquid standard			
	Acetone	Isopropanol	Methanol	Ethylene-glycol
ε'	0.4243	0.5173	0.4734	0.4420
ε''	0.4024	0.7505	0.3337	0.3354

calculations of ε' were obtained for a range of d, from $d = 0$ to $d = 8$ mm. A straight line was fitted to the first nine numerical data from $d = 0$ with $R^2 > 0.99$ and the whole set of numerical data were fitted to a 5th degree polynomial in order to compute the distance to the straight line. According to Fig. 8, a field penetration depth of 1.5 mm was obtained. This procedure was repeated for other frequencies and a slight reduction of the field penetration depth was found as the frequency increased. In Table 4, the field penetration depth at several frequencies is summarized. This finding supports the approximate experimental estimation for the same OE probe determined in González-Teruel et al. (2021) and confirms it is limited to be used only with fine grained media.

3.3. Complex permittivity of soils and water content

In Fig. 9, the complex permittivity of the three soils tested is presented for a selection of water contents from dry to water-saturated states. The data shown are limited to the most accurate bandwidth defined in Section 2.1.2., i.e. 50–700 MHz. The three soils show dielectric dispersion as they become wetter, especially below 300 MHz, where Maxwell-Wagner and other polarization mechanisms show up. This contrasts with the lack of dispersion reported for non-conductive coarse grained soils or talc (González-Teruel et al., 2020; Heimovaara et al., 1994; Szerement et al., 2020). No differences in dielectric dispersion for ε' were observed between the soils tested, even though for clay loam and silt greater ε' values than that for sandy clay loam are reached for similar water contents. Yet, in the case of ε'', the sandy clay loam soil shows much greater dispersion than that of clay loam and silt, which can be attributed to a larger EC, according to the soils characterization presented in Table 1. Special consideration should be given to Fig. 9b, where unsaturated wet samples of the sandy clay loam soil show

higher ε'' values than that of the saturated one, although it should be mentioned that there are differences in ρ_b between the samples, so that for the saturated one ($\theta_v = 0.43$), ρ_b was 1.57 g/cm^3 and for the samples with $\theta_v = 0.35$ and $\theta_v = 0.3$, ρ_b was 1.29 and 1.17 g/cm^3, respectively. Therefore, a greater ρ_b led to lower ε'' under the described circumstances. In contrast, ε' shows a directly proportional relationship with θ_v in all cases, regardless of ρ_b.

The dispersion of the soils tested, especially below 300 MHz, where the vast majority of capacitive and impedance-based soil moisture sensors operate, evidences the impact of EM frequency at which the permittivity is measured and the effect that physical variables such as EC, ρ_b or texture, among others, can have on the dielectric properties of the soil, in such a way that they influence the soil permittivity-moisture relation. In Fig. 10 presents the ε' relationship between 70 and 500 MHz and θ_v for the three soils tested. The ρ_b of the samples is represented according to a colour scale and the Topp et al., (1980) general equation for mineral soils is also presented for comparison. Due to the phase configuration of soils and their aggregation properties, as the water content increases, higher densities were achieved. All three soils fit well to Topp et al.'s curve for the 500 MHz frequency. In general, it is observed that for low θ_v values, which are intrinsically associated with low ρ_b values (<1.3 g/cm^3), the permittivity is slightly below Topp et al.'s curve. In all three soils there is a θ_v threshold above which the measured permittivity is over Topp et al.'s curve. However, in water-saturated or nearly water-saturated samples, high compaction (>1.45 g/cm^3) brings the permittivity values back below Topp et al.'s curve.

In the case of ε' values measured at 70 MHz, these show a shift with respect to those measured at 500 MHz as a consequence of the dielectric dispersion shown in Fig. 9. This shift, which locates the data at 70 MHz above Topp's curve in almost all cases, is more pronounced as soil moisture increases. For dry and nearly dry conditions ($\theta_v < 0.1$), practically no shift is observed in the sandy clay loam soil, unlike in the clay loam and silt soils. Several polarization mechanisms can appear simultaneously in this bandwidth (Hasted, 1973), the discrimination of their contributions being a matter of ongoing debate and beyond the scope of this article.

Table 4

Effective EM field penetration depth of the OE probe at different EM frequencies.

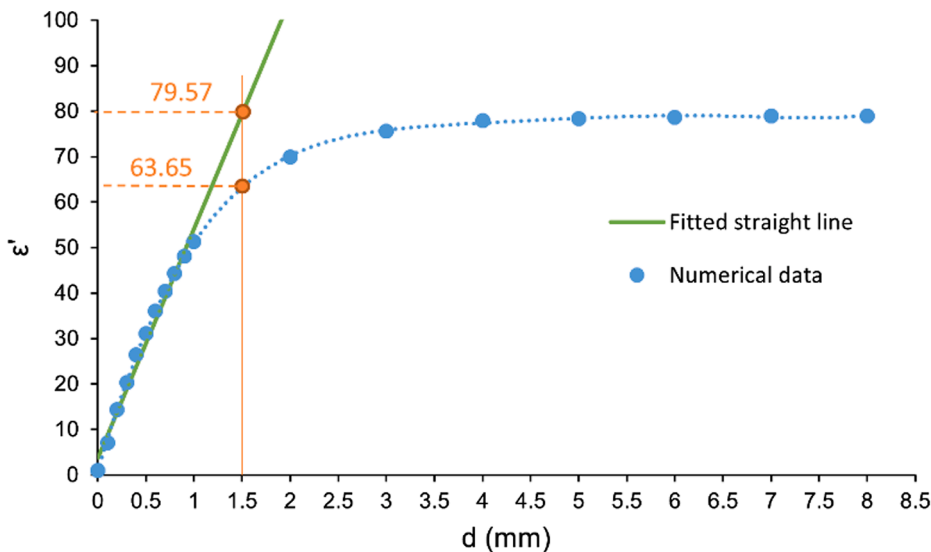| Frequency (MHz)	100	300	500	700	900
Field penetration depth (mm)	1.5	1.39	1.31	1.30	1.30

Fig. 8. Example of effective field penetration depth determination from numerical ε' calculations at 100 MHz.
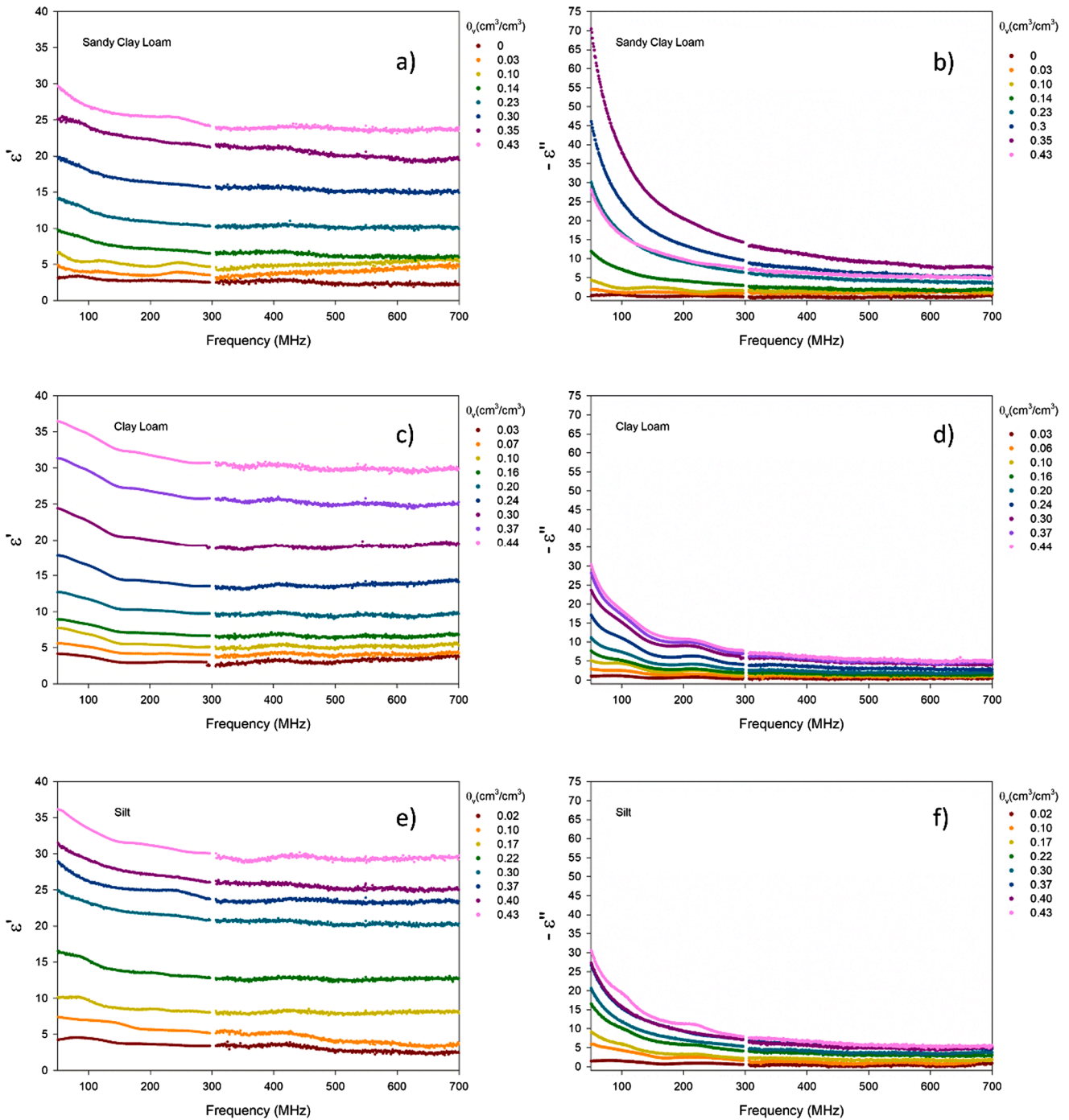
Fig. 9. ε' (a, c, e) and ε'' (b, d, f) of sandy clay loam, clay loam and silt soils at 23 °C determined with the nanoVNA at different water contents.

4. Conclusions

The main aim of this work was to evaluate the nanoVNA, a low-cost, open-source, handheld VNA, for the determination of the broadband complex permittivity of porous media to be applied to soil characterization from 1-port reflection measurements. Additionally, the feasibility of using a self-manufactured open-ended coaxial probe on granular media, already tested on liquids, was assessed. The nanoVNA performance was evaluated on reference dielectric liquids and compared to that of a commercial device, showing comparable accuracy in the bandwidth of comparison (1–500 MHz). Therefore, the nanoVNA was demonstrated to be as accurate as a commercial VNA to determine the complex permittivity of dielectric media, making it suitable and reliable

for use in spectroscopic characterization studies. This makes broadband dielectric measurements in a limited bandwidth more affordable for limited budgets.

When applying the OWL empirical calibration method to estimate the complex permittivity from the $S_{11}*(f)$ with the open-ended coaxial probe, a RMSE of 0.6029 and 0.5482 was obtained for ε' and ε'', respectively, with the nanoVNA, whereas 2.4297 and 2.6840 was obtained with the commercial device on predicting the complex permittivity of organic liquids by using methanol as the Liquid standard in the calibration. The nanoVNA showed limited accuracy beyond 700 MHz as a consequence of noisy S11* measurements. Additionally, the combination of open-ended coaxial probe, VNA and OWL calibration method is limited below 50 MHz, since the real part of $S_{11}*(f)$ tends to be close to
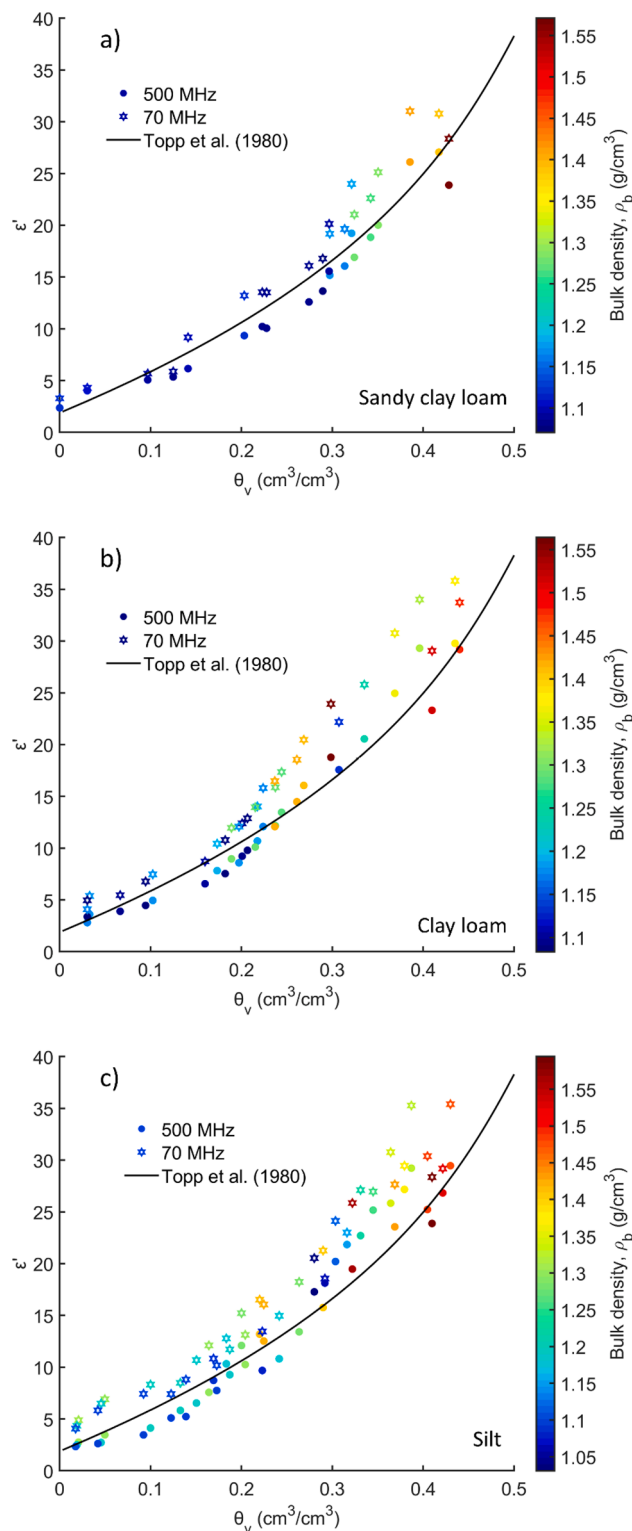
Fig. 10. Dielectric response (ε') of sandy clay loam (a), clay loam (b) and silt (c) soils at 70 and 500 MHz as a function of water content and bulk density at 23 °C determined with the nanoVNA, with a solid line showing the standard empirical calibration for mineral soils (Topp et al., 1980).

1 and the imaginary part close to 0 for every non-conducting material, reducing the sensitivity in this bandwidth. Furthermore, non-conducting organic liquids are normally used as Liquid standards in the OWL calibration, so that the model is less effective when estimating the complex permittivity of conducting materials below approximately 50 MHz.

Thus, the reliable operating bandwidth of the nanoVNA together with the open-ended coaxial probe and the OWL calibration method was determined to be from 50 to 700 MHz. Experiments with conducting liquids such as salt solutions or metallic paints are intended for future work. Alternatively, with an accurate model of the probe, countless artificial material data with the desired dielectric properties could be obtained from FEM simulations, which could be used as a basis for the development of a new model.

To evaluate the feasibility of using the self-manufactured open-ended coaxial probes presented in this study for the dielectric characterization of granular media, we focused on the EM field penetration depth of the probe. The probe was simulated using FEM software and, following the experimental method proposed by (Meaney et al., 2016), the field penetration depth of the probe was determined to be 1.5 mm at 100 MHz, decreasing progressively to 1.3 mm at 900 MHz. To obtain representative measurements from soils, soil material below 0.2 mm were used in order to provide at least 7–8 soil particles vertically in the bulk measurement. The EM field penetration depth of the OE probe has been demonstrated to be limited and we recommend granular samples of diameter below 0.2 mm be used for consistent bulk measurements. In future work, new designs are needed to extend the probe's depth and volume of influence.

The complex permittivity of three mineral soils of varied texture was determined in the 50–700 MHz bandwidth with the nanoVNA and the self-manufactured coaxial open-ended probe for a range of water contents from dry to saturated conditions and for a range of bulk densities between 1 and 1.57 g/cm^3. Dielectric dispersion was observed in the three soils. Insignificant differences for the dielectric dispersion were found between the soil textures tested in terms of ε', whereas in terms of ε'', the sandy clay loam soil showed much greater dispersion than that of the clay loam and silt soils due to a greater EC. This dielectric dispersion leads the low-frequency permittivity to move away from Topp et al.'s reference equation. This highlights the need to take into account the operating EM frequency of soil moisture sensors when calibrating and that the direct use of Topp et al.'s equation with sensors operating at EM frequencies well below the traditional 1000 MHz TDR technique, leads to shifted estimation of water content in soils with dielectric dispersion.

Bulk density is a factor on which the soils dielectric response has been shown to depend as well, but for the soils tested and in the analysed bandwidth, no pattern was observed in the dielectric spectrum that would allow dissociating the effect of water content and density on complex permittivity. Once the measurement set presented in this study has been validated, future work is expected to expand the data set with a greater variety of textures and physicochemical parameters, such as EC or temperature, which will allow a more exhaustive spectroscopic analysis in search of dispersion patterns that allow indirect estimation of physically-based porous medium parameters.

CRediT authorship contribution statement

Juan D. González-Teruel: Conceptualization, Methodology, Software, Formal analysis, Investigation, Data curation, Writing – original draft, Funding acquisition. **Scott B. Jones:** Conceptualization,

Methodology, Validation, Writing – review & editing, Supervision. **David A. Robinson:** Methodology, Validation, Writing – review & editing, Supervision. **Jaime Giménez-Gallego:** Investigation, Writing – review & editing. **Raúl Zornoza:** Resources, Writing – review & editing. **Roque Torres-Sánchez:** Conceptualization, Resources, Writing – review & editing, Supervision, Project administration, Funding acquisition.

Declaration of Competing Interest

The authors declare that they have no known competing financial interests or personal relationships that could have appeared to influence the work reported in this paper.

Acknowledgments

References

Anjos, L., Gaistardo, C., Deckers, J., Dondeyne, S., Eberhardt, E., Gerasimova, M., Harms, B., Jones, A., Krasilnikov, P., Reinsch, T., Vargas, R., Zhang, G., 2015. World reference base for soil resources 2014 International soil classification system for naming soils and creating legends for soil maps, in: Schad, P., Van Huyssteen, C., Micheli, E. (Eds.), . FAO, Rome (Italy).

ASTM, 2018. ASTM D1193 - 06(2018), Standard Specification for Reagent Water, in: ASTM International. www.astm.org, West Conshohocken, PA. https://doi.org/10.1520/D1193-06R18.

Bore, T., Schwing, M., Llano Serna, M., Speer, J., Scheuermann, A., Wagner, N., 2018. A new broadband dielectric model for simultaneous determination of water saturation and porosity. IEEE Trans. Geosci. Remote Sens. 56 (8), 4702–4713. https://doi.org/10.1109/TGRS.2018.2835447.

Buckley, F., Maryott, A.A., 1958. Circular of the Bureau of Standards no. 589: tables of dielectric dispersion data for pure liquids and dilute solutions.

cho45 (Satoh, Hiroh) · GitHub [WWW Document], n.d. URL https://github.com/cho45/ (accessed 1.29.21).

Cole, K.S., Cole, R.H., 1941. Dispersion and absorption in dielectrics I. Alternating current characteristics. J. Chem. Phys. 9 (4), 341–351. https://doi.org/10.1063/1.1750906.

Cross, J.D., 2014. Low-frequency electromagnetic fields for the detection of buried objects in the shallow sub-surface. University of Birmingham, Birmingham.

Dalton, F.N., Herkelrath, W.N., Rawlins, D.S., Rhoades, J.D., 1984. Time-domain reflectometry: Simultaneous measurement of soil water content and electrical conductivity with a single probe. Science (80-.) 224 (4652), 989–990.

Davis, J.L., Chudobiak, W.J., 1975. In situ meter for measuring relative permittivity of soils. Geol. Surv. Canada 75, 75–79.

Debye, P., 1929. Polar Molecules. Dover Publications Inc, New York.

Demontoux, F., Wigneron, J., Mialon, A., Mavrovic, A., Roy, A., Kerr, Y., 2021. A low cost dielectric spectroscopy instrument dedicated to in-situ soil permittivity profile mapping 6198–6201. https://doi.org/10.1109/IGARSS47720.2021.9554253.

edy555 (TT) · GitHub [WWW Document], n.d. URL https://github.com/edy555/ (accessed 1.29.21).

Estevez, R., Jones, S.B., 2009. Frequency Domain Soil Moisture Determination Using Bilinear Analysis with an Open-Ended Dielectric Probe, in: 2009 Reno, Nevada, June 21 - June 24, 2009. American Society of Agricultural and Biological Engineers, St. Joseph, MI, pp. 5964–5981. https://doi.org/10.13031/2013.27297.

García-Baños, B., Catalá-Civera, J.M., Canós, A.J., Peñaranda-Foix, F., 2005. Design rules for the optimization of the sensitivity of open-ended coaxial microwave sensors for monitoring changes in dielectric materials. Meas. Sci. Technol. 16 (5), 1186–1192. https://doi.org/10.1088/0957-0233/16/5/019.

GitHub - hugen79/NanoVNA-H [WWW Document], n.d. URL https://github.com/hugen79/NanoVNA-H (accessed 1.29.21).

GitHub - NanoVNA-Saver [WWW Document], n.d. URL https://github.com/NanoVNA-Saver/nanovna-saver (accessed 7.1.21).

González-Teruel, J.D., Jones, S.B., Giménez-Gallego, J., Robinson, D.A., Lozano-Guerrero, A.J., Torres-Sánchez, R., 2021. Evaluating a low-cost self-manufactured Coaxial Open-Ended Probe for the Measurement of the Complex Permittivity of Granular Media, in: Daschner, F., Höft, M. (Eds.), 13th International Conference on Electromagnetic Wave Interaction with Water and Moist Substances (ISEMA). IEEE, Kiel, Germany, pp. 94–99.

González-Teruel, J.D., Jones, S.B., Soto-Valles, F., Torres-Sánchez, R., Lebron, I., Friedman, S.P., Robinson, D.A., 2020. Dielectric Spectroscopy and Application of Mixing Models Describing Dielectric Dispersion in Clay Minerals and Clayey Soils. Sensors 20, 6678. https://doi.org/10.3390/s20226678.

Gregory, A.P., Clarke, R.N., 2012. Tables of the Complex Permittivity of Dielectric Reference Liquids at Frequencies up to 5 GHz.

Gregory, A.P., Clarke, R.N., 2007. Dielectric metrology with coaxial sensors. Meas. Sci. Technol. 18 (5), 1372–1386. https://doi.org/10.1088/0957-0233/18/5/026.

Hasted, J.B., 1973. Aqueous Dielectrics. Chapman and Hall Ltd., London.

Havriliak, S., Negami, S., 1967. A complex plane representation of dielectric and mechanical relaxation processes in some polymers. Polymer (Guildf) 8, 161–210. https://doi.org/10.1016/0032-3861(67)90021-3.

Heimovaara, T.J., Bouten, W., Verstraten, J.M., 1994. Frequency domain analysis of time domain reflectometry waveforms: 2. A four-component complex dielectric mixing model for soils. Water Resour. Res. 30 (2), 201–209. https://doi.org/10.1029/93WR02949.

Hoekstra, P., Delaney, A., 1974. Dielectric properties of soils at UHF and microwave frequencies. J. Geophys. Res. 79 (11), 1699–1708.

Kaatze, U., 2013. Measuring the dielectric properties of materials. Meas. Sci. Technol. 24 (1), 012005. https://doi.org/10.1088/0957-0233/24/1/012005.

Kaatze, U., 1989. Complex permittivity of water as a function of frequency and temperature. J. Chem. Eng. Data 34 (4), 371–374. https://doi.org/10.1021/je00058a001.

Kraszewski, A., Stuchly, M.A., Stuchly, S.S., 1983. ANA Calibration Method for Measurements of Dielectric Properties. IEEE Trans. Instrum. Meas. 32 (2), 385–387. https://doi.org/10.1109/TIM.1983.4315084.

Kupfer, K., 2004. Electromagnetic Aquametry. Springer, Weimar, Germany.

Loewer, M., Igel, J., Minnich, C., Wagner, N., 2016. Electrical and Dielectric Properties of Soils in the mHz to GHz Frequency Range, in: 11th International Conference on Electromagnetic Wave Interaction with Water and Moist Substances (ISEMA). Florence.

Marsland, T.P., Evans, S., 1987. Dielectric measurements with an open-ended coaxial probe. IEE Proc. H Microwaves, Antennas Propag. 134, 341–349. https://doi.org/10.1049/ip-h-2.1987.0068.

Meaney, P.M., Gregory, A.P., Seppala, J., Lahtinen, T., 2016. Open-Ended Coaxial Dielectric Probe Effective Penetration Depth Determination. IEEE Trans. Microw. Theory Tech. 64, 915–923. https://doi.org/10.1109/TMTT.2016.2519027.

Mosig, J.R., Besson, J.-C., Gex-Fabry, M., Gardiol, F.E., 1981. Reflection of an Open-Ended Coaxial Line and Application to Nondestructive Measurement of Materials. IEEE Trans. Instrum. Meas. IM-30 (1), 46–51. https://doi.org/10.1109/TIM.1981.6312437.

NanoVNA | Very tiny handheld Vector Network Analyzer [WWW Document], n.d. URL http://nanovna.com/ (accessed 1.29.21).

Qiwei, Z., Faiz Zainuddin, M., Fahad Ahmad, A., Obays, S.J., Abbas, Z., 2019. Development of an Affordable Soil Moisture Sensor System with Mini-VNA Tiny and Smartphone. Pertanika J. Sci. Technol 27, 1121–1129.

Reistad, J., 2018. A compact portable resonance probe system for in situ measurements of snow conditions. UiT Norges arktiske universitet.

Ren, T., Ochsner, T.E., Horton, R., 2003. Development of Thermo-Time Domain Reflectometry for Vadose Zone Measurements. Vadose Zo. J. 2 (4), 544–551. https://doi.org/10.2136/vzj2003.5440.

Skierucha, W., Walczak, R., Wilczek, A., 2004. Comparison of Open-Ended Coax and TDR sensors for the measurement of soil dielectric permittivity in microwave frequencies. Int. Agrophysics 18, 355–362.

Skierucha, W., Wilczek, A., 2010. A FDR Sensor for Measuring Complex Soil Dielectric Permittivity in the 10–500 MHz Frequency Range. Sensors 10, 3314–3329. https://doi.org/10.3390/s100403314.

Stuchly, M.A., Brady, M.M., Stuchly, S.S., Gajda, G., 1982. Equivalent Circuit of an Open-Ended Coaxial Line in a Lossy Dielectric. IEEE Trans. Instrum. Meas. IM-31 (2), 116–119. https://doi.org/10.1109/TIM.1982.6312533.

Szerement, J., Saito, H., Furuhata, K., Yagihara, S., Szypłowska, A., Lewandowski, A., Kafarski, M., Wilczek, A., Majcher, J., Woszczyk, A., Skierucha, W., 2020. Dielectric Properties of Glass Beads with Talc as a Reference Material for Calibration and Verification of Dielectric Methods and Devices for Measuring Soil Moisture. Materials (Basel). 13, 1968. https://doi.org/10.3390/ma13081968.

Tanabe, E., Joines, W.T., 1976. A Nondestructive Method for Measuring the Complex Permittivity of Dielectric Materials at Microwave Frequencies Using an Open Transmission Line Resonator. IEEE Trans. Instrum. Meas. IM-25 (3), 222–226. https://doi.org/10.1109/TIM.1976.6312350.

Topp, G.C., Davis, J.L., Annan, A.P., 1980. Electromagnetic determination of soil water content: Measurements in coaxial transmission lines. Water Resour. Res. 16 (3), 574–582. https://doi.org/10.1029/WR016i003p00574.

Wagner, N., Scheuermann, A., 2009. On the relationship between matric potential and dielectric properties of organic free soils: a sensitivity study. Can. Geotech. J. 46 (10), 1202–1215. https://doi.org/10.1139/T09-055.

Wagner, N., Schwing, M., Scheuermann, A., 2014. Numerical 3-D FEM and Experimental Analysis of the Open-Ended Coaxial Line Technique for Microwave Dielectric Spectroscopy on Soil. IEEE Trans. Geosci. Remote Sens. 52 (2), 880–893. https://doi.org/10.1109/TGRS.2013.2245138.